1   Revision 1

2

3   **Tweed, Twins, and Holes**

4

5   Ekhard K.H. Salje

6   Department of Earth Sciences, Cambridge University, Downing Street, Cambridge CB2 3EQ,

7   UK

8

9

10

11   Abstract

12   Tweed, twin and porous microstructures are traditionally studied in mineralogy to understand the

13   thermal history of minerals, and to identify their properties such as chemical transport and elastic

14   behavior. Recently, the same research area has blossomed in material sciences and physics with

15   the aim to design and build devices that are based on the properties of nano-structures. Only the

16   very existence and the properties of tweed, twins, and holes matters in this quest while the

17   crystalline matrix plays only a minor role in the current search for novel device materials. This

18   development has largely bypassed mineralogists while physicists did not profit from the age-long

19   experience of mineralogists in dealing with such materials.

20   In this *Invited Centennial Article* I will first discuss some key findings and approaches to foster

21   the transfer of ideas in both directions: mineralogists can potentially inspire material scientists

22   while the physics of the fine structure of twin walls and tweed can help mineralogists understand

23   mineral properties in much more detail than hereto possible. Besides the observation that novel

24   physical properties can spring from microstructures, most recent work also includes the

25   dynamics of microstructures under external stress or electric fields. The dynamics is virtually

26   always non-smooth or 'jerky'. One of the best studied jerk distribution is that of collapsing

27   porous minerals under stress, where the main focus of research is the identification of precursor

28   effects as warning signs for larger events such as the collapse of mines, boreholes or even

29   regional earth quakes. The underlying physics is the same as in large earth quakes (which can be

30   modeled but not observed in laboratory experiments). The agreement between laboratory

31   experiments of porous collapse and large scale earth quakes goes well beyond each quake

32   statistics and includes waiting-time distributions and the Omori law of after-shocks. The same

33   approach is used to characterize high-tech materials in aircraft industry and functional materials

34   such as used in electronic memory devices, ferroelectric sensors and non-volatile memories and

35   ferromagnets.

Introduction

36

37   Functional properties at the nano-scale, their statics and dynamics, have been investigated in

38   major research initiatives in several disciplines for over 30 years. The relevant nano-structures

39   are, in order of increasing intrusiveness to the matrix: tweed, (transformation-) twins, and holes,

40   and have been used to develop device materials for industrial applications while they naturally

41   exist in many minerals. Tweed and twins in ferroelastic minerals develop when structural phase

42   transitions occur with a loss of point group symmetry elements, which results in transformation

43   twinning in the low temperature phase (Salje 2012). Tweed represents a 'precursor' for twin

44   boundaries in the low symmetry phase (Bratkovsky et al. 1994a-c, Khachaturian 1983, Parlinski

45   et al 1993, Castan et al. 1991). Holes in porous structures often stem from phase mixtures when

46   one phase has been eliminated or where this phase was a gas, as in the case of volcanic ejecta.

47

48   The existence of microstructures with functional properties has opened a new research field in

49   physics and materials science in which the functionality of a device material is no longer

50   expected to be present in the bulk of the material but located in its nanoscopically small regions

51   such as twin boundaries. This approach is summarized as 'domain boundary engineering' in the

52   physics literature (Salje 2010, Salje and Zhang 2009). Nanostructures have always been a major

53   research topic in mineralogy, simply because they are common in minerals (Figure 1) and it may

54   be possible to reconstruct the thermal history of a mineral by exploring their heterogeneities (

55   e.g. Tullis 1980, David et al. 1995, Vernon and Paterson 2008, Trepman and Stuckhert 2001,

56   Vernon 1999, Zhang et al. 1996, Palmer et al. 1989, Salje and Wruck 1983). However, it has not

57   inspired mineralogists to extend their data to find 'unusual' twin boundaries with functionalities

58   such as conductivity, transport, polarity and magnetism (Figure 2). Synthetic porous structure

3

59   (shown in Figure 3) contain similar functionalities near their extremely extended surfaces. Such

60   materials are omnipresent in high-tech applications from cooking pans, nano-scale chemical

61   mixers and nano-filters to artificial bones. Besides the current focus on this research in physics

62   and materials sciences we find that much of the fundamental descriptive work has already been

63   done in mineralogy, often published in American Mineralogist over more than five decades.

64

65

66   **Tweed and twin structures**

67   Tweed forms when local fluctuations become large and lead to atomic displacements which form

68   interwoven pattern of local strain. The orientation of the strain pattern is usually related to the

69   soft elastic directions of a material. Early structural investigations of martensitic phase

70   transformations revealed a pretransitory phenomena that was sandwiched between the high

71   temperature austenite and low temperature martensite phase regions, over a narrow temperature

72   range near the transition temperature (Tullis 1980, Tsatskis and Salje 1996, Kartha, Castan,

73   Krumhansl and Sethna 1995). Tweed is characterized by a crosshatching in the bright-field

74   images, in which the structures are oriented along particular crystallographic directions, and are

75   up to 100 A in length. Upon approaching the transition temperature on cooling, the tweed

76   structures become increasingly pronounced and eventually evolve into the long-range ordered

77   low temperature martensitic polydomain structure. Bratkovsky et al. (1994 a-c) simulated the

78   ordering of tweed structures into thin microdomains and the subsequent coarsening of the thin

79   microdomains into a more traditional domain structure. Thermodynamic fluctuations were

80   shown to control the geometrical dimensions of the tweed modulations. Texturing and

81   coarsening were controlled by long range elastic strains, which resulted in an ordering of

82   modulated embryonic regions. These simulations revealed a common sequence of domain states

4

83 that can be tuned by varying degrees of elastic ordering, temperature, and defects. Kartha et al.

84 (1995) considered the effect of quenched disorder on the evolution of tweed structures towards

85 the twinned phase. More recently, long-time metastable tweed precursor states have been

86 reinvestigated and are referred to as domain glasses (Salje, Ding and Aktas 2014) and other glass

87 states (Wang et al. 2006).

88

89 Another approach to produce tweed is to increase the twin densities. Increasing the twin

90 boundary density is possible by cold stressing a sample (Ding et al. 2012, Salje et al. 2012). In

91 minerals, this happens via rock mechanics where geological processes lead to stress-induced

92 changes of microstructures. This method has been shown to be more effective for generating

93 twins than thermal quench (Ding et al. 2012). Twin densities can be produced very close to the

94 upper structural limit where spacers between the twin boundaries are ca. 10 w where w is the

95 domain boundary width. With w = 1 nm one expects a lower limit for the bulk spacer of some 10

96 nm. Experimentally distances below 100 nm are commonly observed. The reason for the limit of

97 the boundary density is the competition between tweed and twin structures (Shapiro et al. 1991)

98 because highly dense arrays of twin boundaries easily collapse into the tweed structure. This

99 phenomenon is probably widespread in minerals such as K-feldspar and orthoclase (Fig. 4).

100

101

102

103   The diffraction pattern of tweed is shown on the right side insert of Figure 4, and in Figure 5. It

104 is characterized by a four-armed starfish (or clover or butterfly) patterns. Each of the branches in

105 Figure 5 extends along a direction perpendicular to the modulation wavefront. The intensity

5

106   profile does not show any maxima as expected for incommensurate structures but decays

107   monotonically from the zone center over some 0.1 reciprocal lattice units. This diffraction signal

108   can refer either to static tweed (structural modulation, chemical exsolution, etc.) or dynamic

109   tweed where the pattern fluctuates with time. The latter case of dynamic tweed is often referred

110   to as 'flicker tweed' to indicate that the deformation waves are not pinned but move through the

111   sample. Flicker tweed would not be seen in transmission electron microscopy whereas

112   diffraction measures the autocorrelation (the Patterson function) of the modulation and, thus,

113   detects dynamic tweed.

114

115

116

117   **Functionality**

118

119   Tweed and twin pattern can host properties which do not exist in the bulk. Typical examples are

120   electrical or ionic conductivity, polarity and magnetism. The probably most notable local

121   property is superconductivity in an insolating perovskite, namely WO_3 and its derivatives (Aird

122   and Salje 1998, 2000, Kim et al. 2010) (Figure 6). Another example is the formation of dipolar

123   layers in $CaTiO_3$ (Van Aert et al. 2012, Goncalves-Ferreira et al. 2008) (Figure 7) and $SrTiO_3$

124   (Zykova-Timan and Salje 2014, Salje et al. 2013, Scott et al. 2012, Blinc et al 2005).

125

126   Twin boundaries and tweed represent nanostructures that are predestined to interact with several

127   order parameters (e.g. Salje 1993, 2012, Lottermoser et al.2009). In perovskites this situation is

128   particularly simple: one structural order parameter is often the octahedra tilt Q. The second order

6

129 parameter describes the off-centering of the octahedraly coordinated cation. The octahedral tilt

130 reduces the off-centering of the atom from the octahedral midpoint. The coupling between the

131 two parameters is hence repulsive. In a Landau potential the coupling term is formulated as

132 $\lambda Q^n P^m$ where the faintness indices n and m are determined by symmetry. The most common

133 coupling scheme (which is always allowed by symmetry) is $n = m = 2$. This coupling is called bi-

134 quadratic and has been analyzed in much detail by Houchmandzadeh et al. (1991) and Conti et

135 al. (2011). Repulsive coupling means $\lambda > 0$ and interfacial functionality means that $P = 0$ in the

136 bulk. With the Landau functional written as

137

138 $L_\lambda(Q,P) = (1 - Q^2)^2 + (1 - P^2)^2 + \lambda Q^2 P^2 - c_\lambda$ (2)

139 $G_{\kappa,\lambda}[Q,P] = \int L_\lambda(Q,P) + |Q'|^2 + \kappa |P'|^2 \ dx$ (3)

140

141 where the dash means the first spatial derivative of Q or P, respectively. The full phase diagram

142 of this potential was derived by Conti et al. (2011) and is shown in Figure 8. Here we concentrate

143 on phases with $P = 0$ in the bulk. This condition is met inside the interval $\lambda > 2$ below the bend

144 curve expanding to larger values of λ. This condition means that the repulsive force needs to be

145 large enough to destroy P in the bulk but not in the twin boundary and that the intrinsic wall

146 thicknesses κ limits the value of λ to $\lambda < 2 + 4/\kappa$. In these cases the twin boundary in Q will

147 always host a local parameter P which represents the functionality of the wall.

148 Other coupling schemes were explored by Salje and Carpenter (2011) and Pottiger and Salje

149 (2014). Gradient coupling (Zhao et al. 2015) will not be considered in this report. In tweed

150 structures, a similar coupling scheme applies and has been described by Salje and Aktas (2014).

151

Collapse: the hole story

152

153 The dynamics of functional tweed and twin boundaries are surprisingly un-smooth (Salje and

154 Dahmen 2014). When external forces are applied to change the domain pattern, the pattern often

155 reacts by jerky movements and only in the case of very mobile patterns in adaptive structures

156 (Viehland and Salje 2014) are such 'jerks' or spikes replaced by a continuous movement. The

157 origin of jerks is sometimes related to pinning of microstructures to impurities - while Peierls

158 pinning is rather uncommon (Goncalves-Ferreira 2010, Lee et al. 2006). Impurity pinning is not

159 the only or even the most common reason, however, because microstructures also jam. Jamming

160 means that the movement of part of the pattern is hindered by other parts of the pattern. No

161 defects or impurities are needed for this mechanism (Salje et al. 2011). Jamming produces

162 'crackling noise' which is a sequence of jerks which follow an extremely well-defined statistical

163 pattern which is very close to the Gutember-Richter law in earth quakes (Setna et al. 2001, Salje

164 and Dahmen 2014, Baro et al. 2013). The concept of jerks and crackling noise has hence been

165 around for a long time, but has hardly ever been applied to minerals. Starting with Barkhausen

166 analysis of magnetization jumps in slowly magnetized ferromagnets, it was generalized to

167 'crackling noise' because it was found that similar phenomena are much more wide- spread than

168 in magnetism alone (Setna et al. 2001), including the crackling of a log fire which originated the

169 name. Other fields that show crackling noise include: granular materials (Salje 2012, Jaeger et a.

170 1996, Dahmen et al. 2011), collapse of porous materials (Salje et al. 2011, 2013,   Baró et al.

171 2013, Ben-Zion et al. 2011), plasticity in small crystals (Zaiser 2006, Dahmen et al. 2009.),

172 change in the co-existence interval of stepwise structural phase transitions (Salje 2012, Romero,

173 Manchado, Martin-Olalla, Gallardo, Salje, 2011), transitions in Mott insulators (Lashley et al.

174 2014), and decision-making processes (Friedman et al. 2012). Materials applications extended

8

175   initially in martensitic alloys, and magnetic materials (for nondestructive materials testing),

176   while similar phenomena were well studied in geophysical applications such as the statistical

177   analysis of in earth quakes.

178

179   Many systems with crackling noise show similar statistics. For example it has been shown

180   experimentally and theoretically that the size distribution of magnetization avalanches of soft

181   magnetic materials, observed as Barkhausen noise, decays with the same power law as the slip-

182   size distribution of slowly compressed samples (Zaiser 2006, Dahmen et al. 2009, Galam 1997,

183   Miguel and Zapperi 2006, Tsekenis et al. 2013, Dimiduk et al. 2006, Friedman et al. 2012,

184   Harrison and Salje 2010, 2011, Csikor et al. 2007). Renormalization group calculations

185   suggest that on long length scales the systems flow to the same fixed point under coarse graining,

186   which suggests that their scaling behavior on long length scales is the same (Richeton et al.

187   2005, Sethna et al. 2001). In fact, all systems described by the well known "interface depinning

188   universality class" flow to the same fixed point as these two systems (Zaiser 2006,

189   Richeton,Weiss,Louchet 2005). Major open questions concern the size of the underlying

190   universality class, i.e. how many systems show the same crackling noise statistics.

191

192   For mineralogists the outstanding system where such universal jerks properties can be measured

193   with great accuracy is the collapse of porous minerals. These can serve as a model system for a

194   wide variety of systems ranging from earth-quakes to ferroelectric device materials and poling of

195   magnetic minerals in paleomagnetism. Porous minerals are important in their own right too: they

196   are widely used in filtering, separation, medical transplants and others (Kim et al. 2012, Petri et

197   al. 2008, Gallardo et al. 2010, Salje et al. 2009). Understanding porous materials remains one

198   of the great challenges in mining, building industry and geology. Mining is often done in

199   environments containing porous mineral assemblies (Salje et al. 2013, Manosa et al. 2000),

200   including goethite, pyrite and coal, which may lead to serious accidents when landslides occur in

201   open mining or when mining shafts collapse. Such catastrophic events are sometimes announced

202   by acoustic precursors of the collapse (Salje et al 2013, Zhao et al. 2013, Salje et al. 2013,

203   Castillo-Villa et al. 2013). The typical failure under shear stress is that a porous material 'snaps'

204   when exposed to the critical shear stress. Crack propagation is fast and few intermediate states

205   are observed at low temperatures. Snapping becomes more viscous for torsion pendulum

206   experiments at high temperatures near the melting point where grain boundary sliding and

207   dislocation creep become dominant (e.g., Gibson, Ashby 1999). In a recent study, Salje et al.

208   (2011) used a porous SiO_2 glass material (Vycor) to show that avalanches produced by

209   compression follow almost perfect power law statistics ('crackling noise') with characteristic

210   critical exponents similar to those measured in mechanical instabilities in martensites and

211   ferroelastic materials, critical dynamics in micro fracturing (Kashef et al. 2011), and spontaneous

212   acoustic emission in volcanic rocks. This has put the problem of understanding the failure of

213   porous materials under compression within the scenario of crackling noise and avalanche

214   criticality.

215

216   The acoustic activity is not restricted to the time interval of the collapse but occurs over the

217   whole time span of the experiment. Even at times after the collapse, the debris still contains

218   intact, porous regions which collapse when the stress is increased further. In the log-log plot in

219   Figure 11 the energy distribution P(E) of jerks is shown as function of the energy E. As can be

220 seen the histograms are quite linear in this plot. This suggests again that the distribution of

221 energies follows a power law:

222

223 $\quad P(E)\, dE \quad \sim \quad E^{-\varepsilon} / E_{min}{}^{1-\varepsilon}$

224

225 where E_{min} is a lower cutoff used for normalization. The lines in Figure 11 are guides to the eye.

226 They reveal the increasing value of the exponent ε with porosity. Interestingly the Vycor sample

227 with a porosity of 40% shows features similar to those of the least porous goethite samples: a

228 similar noise spectrum with no detectable noise gap after the major collapse. The major

229 difference between goethite and Vycor is that the Vycor sample shows a power law distribution

230 of the acoustic emission spectra over a very large interval of six orders of magnitude while the

231 experimentally accessible interval in goethite is smaller. Furthermore the power-law exponents

232 for goethite are larger than the value of 1.39 of the Vycor sample. Otherwise, it appears that the

233 noise detection, and hence the analysis of potential early warning noise before collapses, is

234 independent of the composition of the material and depends only on its porosity. Nataf et al.

235 (2014) investigated SiO_2- based materials including sandstone and synthetic glasses and found

236 that the noise statistics are very similar for all of them. The close connection to the earth-quake

237 statistics, including waiting times and after-shock probabilities, have led to the notion that earth

238 quakes (or their proxys) can be investigated experimentally (and not just by simulation) in the

239 laboratory (Biswas et al. 2013, Main et al. 1989, Baro et al. 2013, Castillo-Villa et al. 2013).

240

241

242 **Resonant piezoelectric spectroscopy**

243   Polar behavior (ferroelectric/piezoelectric/ferrielectric behavior) in tweed, twin walls, and near

244   surfaces in porous minerals relates to a very small number of atoms which constitute a tiny

245   percentage of the sample (typically 0.1 ppm). This means that their piezoelectric signal is quite

246   weak and a very sensitive experimental technique is needed for its investigation. One of the best

247   tools for the detection of weak polarity is second harmonic generation microscopy (SHG).

248   Second-harmonic generation has been reviewed as a tool for studying polarity and electronic and

249   magnetic structures of crystals in Fiebig et al. (2005). However, one has to be careful with the

250   interpretation of SHG data because local defects can easily induce SHG signals (Bleser et al.

251   1994, Meier et al. 2010, Becker and Bohatý 2010, Lottermoser et al. 2009, Frey and Payne

252   1996, Yokota et al. 2014).

253

254   Recently a new experimental technique, resonant piezoelectric spectroscopy (RPS), has been

255   introduced (Salje et al. 2013, Aktas et al. 2013, Aktas et al. 2013). The experimental arrangement

256   for resonant piezoelectric spectroscopy (RPS) is shown in Figure 12. If the sample is

257   piezoelectric, the AC voltage applied between two parallel surfaces of the sample leads to the

258   oscillation of domain boundaries. This oscillation creates strain fields proportional to the electric

259   field and forms elastic waves propagating in the sample. If the frequency of the elastic wave

260   corresponds to one of the natural frequencies of the sample, it becomes resonant and its

261   amplitude increases drastically. This mechanical resonance condition makes RPS highly

262   sensitive to polar ordering even at nano scales. The detection of resonant elastic standing waves

263   (i.e., mechanical resonances), is then achieved using a piezoelectric detector attached to one end

264   of an alumina rod which transmits any signal received from the sample to the piezoelectric

265   detector. Note the similarity between the experimental arrangements of RPS and RUS (Salje et

266   al. 2013). In RUS, elastic waves are generated mechanically by the application of an AC voltage

267   across a piezoelectric transducer (the top transducer in Figure 12). In RPS the AC voltage is

268   applied across the sample, which will generate elastic waves only if the sample, locally or

269   macroscopically, shows piezoelectric behavior.

270

271   As an example, we performed RPS measurements on quartz with an AC voltage of 20 V

272   applied across two parallel surfaces in the basal plane of the sample. Segments of spectra

273   collected between 300 K and 1050 K are shown in Figure 13. The spectrum shown in green is

274   assumed to have been collected at the α-β transition at T_c = 846 K, where α corresponds to the

275   low temperature phase with the point group 32 while β is the high-temperature phase that

276   belongs to the point group 622. There are mechanical resonances peaks both below and above T_c,

277   which indicates piezoelectricity in both phases. This is consistent with the symmetry properties

278   of the α and β phases. In the α phase the piezoelectric coefficients d_{11} and d_{14} are active, while in

279   the β phase only d_{14} is active (Ohno, Harada, Yoshitomi 2006). Monotonous temperature

280   behavior of resonance amplitudes at T_c implies that resonances are excited mainly by the

281   piezoelectric coefficient d_{14}. Elastic properties of quartz have been determined in great detail

282   elsewhere (Carpenter et al. 1998) and will not be discussed in this review. However, it is worth

283   noting that in the spectra shown in Figure 12 resonances the frequencies of which do not change

284   significantly with temperature belong to alumina rods. Other resonances which show a frequency

285   dip at T_c , belong to the quartz sample. The square of a resonant frequency is proportional to the

286   effective elastic constant associated with the resonance. Therefore, the observed softening in

287   resonant frequencies is in agreement with earlier reports of the co/elastic nature of quartz.

288

13

289

290   The same experimental method has now been employed to observed polar domain walls. RPS

291   spectra of paraelectric $SrTiO_3$ were collected between 15 K and 100 K and are shown in Figure

292   14. Upon cooling, peaks associated with mechanical resonances of the $SrTiO_3$ sample appear

293   below 80 K, which is well below the ferroelastic transition temperature T_c = 105 K. As the

294   temperature is reduced, the amplitudes of resonance peaks reach their maximum values below 40

295   K. Considering that bulk $SrTiO_3$ shows no ferroelectric or piezoelectric behavior, the observed

296   piezoelectric behavior indicates that the twin walls become polar below 80 K. The gradual

297   increase in amplitudes implies that piezoelectricity inside the twin walls, increases upon cooling

298   and leads to the mobility of twin walls and hence proves the functionality of twin walls in

299    $SrTiO_3$. RPS is hence shown to be sensitive enough to observe these microstructure-related

300   polarities even when the number of atoms in the polar state is very small. It is a method which

301   may be able to find such states in minerals where polarity has not been reported before. The

302   polartity of twin boundaries of $SrTiO_3$ has been confirmed by computer simulations (Zykova–Timan and

303   Salje 2014) where the local structure is not simply amd array of dipoles in the wall but contains vortices

304   which lead to rotations of ferroelectric dipoles, as shown in Figure 15. It was shown subsequently that

305   these dipoles can be switched by electric fields, which demonstrates that twin boundaries in perovskites

306   structures are indeed functional in several chemical compounds. We expect that more examples will be

307   found in the future with some of these examples coming from mineralogical collections.

308

309   **Implications**

310   The implications of our observations are wide– ranging. First, we cannot take it for granted anymore that

311   ionic transport is dominated by the transport coefficient of the bulk material. Whenever the interfacial

312   density is high, we can short–cut the bulk and transport mainly through the network of interfaces. This

313   effect is even greater when electronic transport, or hole transport, is considered.

314   We have given a general scheme to quantify the coupling between order parameters and other quantities

315   such as polarity and conductivity. These schemes apply to many minerals. While these results will

316   probably not falsify previous results in the mineralogical literature, they add another dimension. Minerals

317   may be high–tech materials, but we simply do not know. We are in a similar situation as in the beginning

318   of research on ferroelectric materials in the 1950s many of the first surveys were conducted in

319   mineralogical collections where minerals were systematically tested for their ferroelectric behavior. Later

320   the same happened for magnetic materials. Today we should test domain boundary for any functional

321   behavior (conductivity, polarity, piezoelectricity, ferroelectricity, magnetism etc.) and also their dynamic

322   behavior. There is a lot to do.

323

326

327

328   References:

329

330   Aird, A., and Salje E.K.H. (2000) Enhanced reactivity of domain walls in with sodium, European

331   Journal Physics, B 15, 205–210.

332

333   Aird, A., and Salje, E.K.H. (1998) Sheet superconductivity in twin walls: experimental evidence,

334   Journal Physics Condenseed Matter, 10, L377.

335

336   Aktas, O., Carpenter, M.A. and Salje, E.K.H. (2013) Polar precursor ordering in BaTiO3

337   detected by resonant piezoelectric spectroscopy, Applied Physics Letters, 103, 142902.

338

339   Aktas, O., Salje, E. K. H., Crossley, S., Lampronti, G. I., Whatmore, R. W., Mathur, N. D. and

340   Carpenter, M. A. (2013) Ferroelectric precursor behavior in PbSc0.5Ta0.5O3 detected by field-

341   induced resonant piezoelectric spectroscopy, Physical Review, B 88, 174112.

342

343   Aufort, J., Aktas, O. and Salje, E.K.H. (2014) Resonant piezoelectric spectroscopy in SiO2-

344   based materials, submitted American Mineralogist.

345

346   Baró, J., Corral, A., Illa, X., Planes, A., Salje, E.K.H., Schranz, W., Soto-Parra, D.E., and Vives,

347   E. (2013) Statistical Similarity between the Compression of a porous material and earthquakes.

348   Physical Review Letters, 110, 088702.

349

16

350   Becker P., and Bohatý L. (2010) Second harmonic generation on incommensurate structures:

351   The case of multiferroic $MnWO_4$, Physical Review, B 82, 155112.

352

353   Ben-Zion, Y., Dahmen, K.A., and Uhl, J.T. (2011) A Unifying Phase Diagram for the Dynamics

354   of Sheared Solids and Granular Materials, Pure Applied Geophysics 168, 2221–37.

355

356   Biswas, S., Ray, P., and Chakrabarti, B. K. (2013) Equivalence of the train model of earthquake

357   and boundary driven Edwards-Wilkinson interface, European Physics Journal, B 86, 388.

358

359   Bleser, T ., Berge, B ., Bismayer, U., and Salje, E.K.H. (1994) The possibility that the optical

360   second-harmonic generation in lead phosphate, Pb3(PO4)2 , is related to structural

361   imperfections, Journal Physics Condensed Matter, 6, 2093-9.

362

363   Blinc, R., Zalar, B., Laguta, V.V., and Itoh,M. (2005) Order-disorder component in the phase

364   transition mechanism of ^{18}O enriched strontium titanate. Physical Review Letters., 94,147601.

365

366   Bratkovsky, A.M., Marais, S.C., Heine, V., and Salje, E. K. H. (1994) The theory of fluctuations

367   and texture embryos in structural phase transitions mediated by strain. Journal Physics

368   Condensed Matter, 6, 3679-3696.

369

370   Bratkovsky, A. M., Salje, E. K. H., and Heine, (1994) V. Overview of the origin of tweed

371   texture, Phase Transitions, 52, 77–83.

372

373   Bratkovsky,A.M., Salje, E. K. H., Marais, S. C., and Heine, V. (1994) Theory and computer

374   simulation of tweed texture. Phase Transitions, 48, 1–13.

375

376   Castan, T., Vives, E., and Lindgard, P.A. (1999) Modeling premartensitic effects in Ni2MnGa: A

377   mean-field and Monte Carlo simulation study, Physical Review, B 60, 7071-7084.

378

379   Castillo-Villa, P. O., Baro, J., Planes, A., Salje, E. K. H., Sellappan, P., Kriven, W. M., and

380   Vives, E. (2013) Crackling noise during failure of alumina under compression: the effect of

381   porosity, Journal Physics Condensed Matter, 25, 292202.

382

383   Carpenter, M.A., Salje, E.K.H., Graeme-Barber, A., Wruck, B., Dove, M.T., and Knight, K.S.

384   (1998) Calibration of excess thermodynamic properties and elastic constant variations associated

385   with the alpha <–>beta phase transition in quartz, American Mineralogist, 83, 2–22.

386

387   Conti,S., Müller,S., Poliakovsky,A., and Salje,E.K.H. (2011) Coupling of order parameters,

388   chirality, and interfacial structures in multiferroic materials, Journal Physics Condensed Matter,

389   23,142203.

390

391   Csikor, F.F., Motz, C., Weygand, D., Zaiser, M., and Zapperi, S. (2007) Dislocation avalanches,

392   strain bursts, and the problem of plastic forming at the micrometer scale, Science, 318, 251–54.

393

394   Dahmen, K.A., Ben-Zion, Y., and Uhl, J.T. (2011) A simple analytic theory for the statistics of

395   avalanches in sheared granular materials, Nature Physics, 7:554–57.

396

397   Dahmen, K.A., Ben-Zion, Y., and Uhl, J.T. (2009) Micromechanical Model for Deformation in

398   Solids with Universal Predictions for Stress-Strain Curves and Slip Avalanches, Physical Review

399   Letters,102, 175501.

400

401   David, F., Walker, F.D.L., Lee, M.R., and Parsons I.(1995) Micropores and micropermeable

402   texture in alkali feldspars, Mineralogical Magazine 59, 505–534 .

403

404   Dimiduk, D.M., Woodward, C., LeSar, R., and Uchic, M.D. (2006) Scale-free intermittent flow

405   in crystal plasticity, Science, 312, 1188–90.

406

407   Ding,X., Zhao, Z., Lookman, T. , Saxena, A., and Salje, E. K. H. (2012) High junction and twin

408   boundary densities in driven dynamical systems, Advanched Materials, 24, 5385–5389.

409

410   Fiebig, M., Pavlov, V.V., and Pisarev, R.V. (2005) Second-harmonic generation as a tool for

411   studying electronic and magnetic structures of crystals: review, Jornal Optical Society America,

412   B 22, 96–118.

413

414   Frey, M. H. , and Payne, D. A. (1996) Grain-size effect on structure and phase transformations

415   for barium titanate, Physical Review, B, 54, 3158–3168.

416

417   Friedman, N., Ito, S., Brinkman, B.A.W., Shimono, M., DeVille, R.L., Dahmen, K. A., Beggs, J.

418   M., and Butler, T. C. (2012a) Universal Critical Dynamics in High Resolution Neuronal

419   Avalanche Data, Physical Review Letters, 108, 208102.

420

421   Friedman, N., Jennings, A.T., Tsekenis, G., Kim, J.Y., Uhl, J.T., Greer, J. R., and Dahmen, K. A.

422   (2012b) Statistics of Dislocation Slip Avalanches in Nanosized Single Crystals Show Tuned

423   Critical Behavior Predicted by a Simple Mean Field Model, Physical Review Letters, 109,

424   095507.

425

426   Galam, S. (1997) Rational group decision making: A random field Ising model at T=O. Physics,

427   A 238, 66–80.

428

429   Gallardo, M.C., Manchado, J., Romero, F.J., Del Cerro, J., Salje, E.K.H., Planes, A., Vives, E.,

430   Romero, R., and Stipcich, M. (2010) Avalanche criticality in the martensitic transition of

431   Cu67.64Zn16.71Al15.65 shape-memory alloy: A calorimetric and acoustic emission study,

432   Physical Review, B 81, 174102.

433   Gibson, L.J., and Ashby, M.F.(1999) Cellular Solids. Cambridge University Press, Cambridge,

434   UK.

435

436   Goncalves-Ferreira, L., Redfern, S.A.T.,Artacho, E., and Salje, E.K.H.(2008) Ferrielectric twin

437   walls in $CaTiO_3$, Physical Review Letters, 101, 097602.

438

439   Goncalves-Ferreira, L., Redfern, S.A.T., Artacho, E., Salje, E.K.H., and Lee, W.T. (2010)

440   Trapping of oxygen vacancies in the twin walls of perovskite, Physial Review,B, 81, 024109.

441

442   Harrison, R.J., and Salje, E.K.H. (2010) The noise of the needle: Avalanches of a single

443   progressing needle domain in LaAlO3, Applied Physics Letters, 97, 021907.

444

445   Harrison, R.J., and Salje, E.K.H. (2011) Ferroic switching, avalanches, and the Larkin length:

446   Needle domains in LaAlO3, Applied Physis Letters, 99, 151915.

447

448   Houchmandzadeh,B.,Lajzerowicz,J., and Salje,E. (1991) Order parameter coupling and chirality

449   of domain walls, Journal Physics Condensed Matter, 3, 5163-5168.

450

451   Jaeger, H., Nagel, S.R., and Behringer, R.P. (1996) Granular solids, liquids, and gases, Review

452   Modern Physics, 66, 1259–73.

453

454   Kampfe,T., Reichenbach, P. , Schroder, M. , Haußmann, A., Eng , L. M. , Woike, T., and

455   Soergel, E. (2014) Optical three-dimensional profiling of charged domain walls in ferroelectrics

456   by Cherenkov second-harmonic generation, Physical Review, B 89, 035314.

457

458   Kashef, S.,Asgari, A., Hilditch, T.B., Yan, W.Y. ,Goel, V.K., and Hodgson, P.D.(2011) Fatigue

459   crack growth behavior of titanium foams for medical applications, Material Science Engineering,

460   A528, 1602–7.

461

462   Kartha,S., Krumhansl, J.A., Sethna, J.P., and Wickham, L.K. (1995) Disorder-driven

463   pretransitional tweed pattern in martensitic transformations, Physical Review, B 52, 803-822.

464

465   Kartha S.,Castan,T., Krumhansl, J.A., and Sethna,J.P. (1991) Spin-glass nature of tweed

466   precursors in martensittic transformations, Physical Review Letters, 67, 3630-3633.

467

468   Khachaturian, A. G.(1983) Theory of Structural Transformations in Solids. Dover Books on

469   Engineering Series. Dover Publications Incorporated, USA.

470

471   Kim, Y., Alexe, M., and Salje, E. K. H. (2010) Nanoscale properties of thin twin walls and

472   surface layers in piezoelectric WO3-x, Applied Physics Letters, 96, 032904.

473

474   Kim J.Y., Gu X., Wraith M., Uhl J.T., Dahmen K.A., and Greer JR. Suppression of Catastrophic

475   Failure in Metallic Glass-Polyisoprene Nanolaminate Containing Nanopillars (2012) Advanced

476   Functional Materials, 22, 1972–80.

477

478   Lashley, J. C.,Gofryk, K.,Mihaila, B.,Smith, J. L., and Salje, E. K. H. (2014) Thermal avalanches

479   near a Mott transition, Journal Physics Condensed Matter, 26, 035701.

480

481   Lee, W. T.,Salje, E. K. H.,Goncalves-Ferreira, L.,Daraktchiev, M., and Bismayer, U. (2006)

482   Intrinsic activation energy for twin-wall motion in the ferroelastic perovskite CaTiO3, Physical

483   Review, B 73, 214110.

484

22

485   Locherer, K.R., Chrosch, J., and Salje, E.K.H. (1998) Diffuse x-ray scattering in WO3, Phase

486   Transitions, 67, 51-63.

487

488   Lottermoser Th., Meier D., Pisarev R. V., and Fiebig M. (2009) Giant coupling of second-

489   harmonic generation to a multiferroic polarization, Physical Review, B, 80, 100101.

490

491   Main I.G., Meredith P.G., and Jones C. (1989) A reinterpretation of the precursory seismic B-

492   value anomaly from fracture-mechanics, Geophysical Journal, 96, 131-138.

493

494   Manosa L., Carrillo L., Vives E., Obrado E., Gonzalez-Comas A., and Planes A. (2000)

495   Acoustic emission at the premartensitic and martensitic transitions of Ni2MnGa shape memory

496   alloy, Materials Science Forum, 327-3, 481–84.

497

498   McLaren A.C., and Fitz Gerald J.D. (1987) Cbed and alchemi investigation of local symmetry

499   and Al, Si ordering in k-feldspars. Physics Chemistry of Minerals, 14, 281–292.

500

501   Miguel M.C., and Zapperi S. (2006) Fluctuations in plasticity at the microscale, Science, 312,

502   1151–52.

503

504   Meier, D. , Leo, N. , Yuan, G. , Lottermoser, Th., Fiebig, M. , Becker, P., and Bohatý, L. (2010)

505   Second harmonic generation on incommensurate structures: The case of multiferroic $MnWO_4$.

506   Physical Review, B, 82, 155112.

507

23

508   Nataf, G.F., Castillo-Villa, P.O., Baro, J., Vives, E., Planes, A., and Salje E.K.H. (2014)

509   Avalanches in compressed porous SiO2-based materials. Physical Review, E **90**, 022405.

510

511   Ohno I., Harada K., and Yoshitomi C. (2006) Temperature variation of elastic constants of

512   quartz across the alpha-beta transition, Physics Chemistry of Minerals, 33,1–9.

513

514   Parlinski,K., Heine, V., and Salje, E.K.H. (1993 a) Origin of tweed texture in the simulation of a

515   cuprate superconductor, Journal Physics Condensed Matter, 5, 497-519.

516

517   Parlinski, K., Salje, E.K.H., and Heine, V. (1993 b)Annealing of tweed microstructure in high Tc

518   superconductors studied by a computer simulation, Acta Metallurgica et Materialia, 41, 839 –

519   847.

520

521   Palmer D.C., Salje E.K.H., and Schmahl W.W. (1989) Phase Transitions in Leucite – X-ray

522   diffraction studies, Physics Chemistry Minerals, 16, 714-719.

523

524   Petri A., Baldassarri A., Dalton F., Pontuale G., Pietronero L., and Zapperi S. (2008) Stochastic

525   dynamics of a sheared granular medium, European Physics Journal, B 64, 531–35.

526

527   Pottiger, H., and Salje, E.K.H. (2014) Twin boundary profiles with linear-quadratic coupling

528   between order parameters. Jounal Physics Condensed Matter, 26, 342201.

529

530   Putnis, A., and Salje, E. (1994) Tweed microstructures: Experimental observations and some

531   theoretical models. Phase Transitions, 48, 85–105.

532

533   Richeton T., Weiss J., and Louchet F. (2005) Breakdown of avalanche critical behaviour in

534   polycrystalline plasticity, Nature Materials, 4, 465–69.

535

536   Romero F.J.,Manchado J., Martin-Olalla J.M.,Gallardo M.C., and Salje E.K.H. (2011) Dynamic

537   heat flux experiments in Cu67.64Zn16.71Al15.65: Separating the time scales of fast and ultra-

538   slow kinetic processes in martensitic transformations, Applied Physics Letters, 99, 011906.

539

540   Salje E.K.H. (1993) Phase transitions in ferroelastic and co-elastic crystals. Cambridge

541   University press, Cambridge UK.

542

543   Salje E. K. H.,Carpenter M. A.,Nataf G. F.,Picht G.,Webber K., Weerasinghe J.,Lisenkov S., and

544   Bellaiche, L. (2013) Elastic excitations in BaTiO3 single crystals and ceramics: Mobile domain

545   boundaries and polar nanoregions observed by resonant ultrasonic spectroscopy, Physical

546   Review, B 87, 014106.

547

548   Salje E.K.H., and Aktas O. (2014) Functional twin boundaries and tweed microstructures: a

549   comparison between minerals and device materials, Mineralogical Magazine , in press,

550

551   Salje, E. K. H., Ding, X. , Zhao, Z. , Lookman, T., and Saxena, A. (2011) Thermally activated

552   avalanches: Jamming and the progression of needle domains, Physical Review, B, 83, 104109.

553

554   Salje E.K.H., Koppensteiner J., Reinecker M., Schranz W., and Planes A. (2009) Jerky elasticity:

555   Avalanches and the martensitic transition in Cu74.08Al23.13Be2.79 shape-memory alloy,

556   Applied Physis Letters, 97, 021907.

557

558   Salje, E. K. H., Aktas, O., Carpenter, M. A., and Scott J.F. (2013) Domains within Domains and

559   Walls within Walls: Evidence for Polar Domains in Cryogenic SrTiO3, Physical Review Letters,

560   111, 247603.

561

562   Salje E.K.H., Lampronti G.I., Soto-Parra D.E., Baró J., Planes A., and Vives E. (2013) Noise of

563   collapsing minerals: Predictability of the compressional failure in goethite mines, American

564   Mineralogist, 98, 609–615.

565

566   Salje EKH. (2012) Ferroelastic Materials, Annual Review Materials Research, 42, 265–83.

567

568   Salje, E.K.H., Ding, X., and Aktas, O. (2014) Domain Glass, Phys. Status Solidi B 1–6, DOI

569   10.1002/pssb.201350242.

570

571   Salje, E. K. H., Ding, X. , Zhao, Z., and Lookman T. (2012) How to generate high twin densities

572   in nano-ferroics: Thermal quench and low temperature shear, Applied Physis Letters, 100,

573   222905.

574

26

575   Salje E. K. H., and Carpenter, M. A. (2011) Linear-quadratic order parameter coupling and

576   multiferroic phase transitions, Journal Physics Condensed Matter, 23, 462202.

577

578   Salje E. K. H., Aktas, O., Carpenter, M. A., and Scott J.F. (2013) Domains within Domains and

579   Walls within Walls: Evidence for Polar Domains in Cryogenic SrTiO3, Physical Review Letters,

580   111, 247603.

581

582   Salje E., Gehlig R., and Viswanathan K. (1978) Structural phase-transitions in mixed crystals

583   WxMo1-xO3, Journal Solid State Chemistry, 25, 239-250.

584

585   Salje E., and Wruck B. (1983) Specific heat measurements and critical exponents of the

586   ferroelastic phase-transition in Pb3(PO4)2 and Pb3 (P—xAsxO4)2 , Physical Review, B 28,

587   6510-6518.

588

589   Salje, E.K.H., and Dahmen, K.A. (2014) Crackling Noise in Disordered Materials, Annual

590   Review of Condensed Matter Physics 5, 233-254.

591

592   Salje, E.K.H. (2010) Multiferroic domain boundaries as active memory devices: Trajectories

593   towards domain boundary engineering. ChemPhysChem, 11, 940–950.

594

595   Salje E.K.H., Soto-Parra D.E., Planes A., Vives E., Reinecker M., and Schranz W. (2011) Failure

596   mechanism in porous materials under compression: crackling noise in mesoporous SiO2,

597   Philosophical Magazine Letters, 91, 554–60.

27

598

599   Salje E., and Zhang, H. (2009) Domain boundary engineering. Phase Transitions, 82, 452–469.

600

601   Schmahl, W. W., Putnis, A., Salje, E. , Freeman, P. , Graeme-Barber, A. , Jones, R., Singh,

602   K. K., Blunt, J. , Edwards, P. P., Loram, J., and Mirza, K. (1989) Twin formation and structural

603   modulations in orthorhombic and tetragonal YBa2(Cu1-xCox)3o7- δ, Philosophical Magazine

604   Letters, 60, 241–248.

605

606   Scott, J. F., Salje, E. K. H., and Carpenter, M. A. (2012) Domain Wall Damping and Elastic

607   Softening in SrTiO3: Evidence for Polar Twin Walls, Physical Review Letters, 109, 187601.

608

609   Sethna, J.P., Dahmen, K.A., and Myers, C.R. (2001) Crackling noise. Nature, 410, 242-250.

610

611   Shapiro,S.M., Yang, B. X., Noda, Y. , Tanner, L. E., and Schryvers D. (1991) Neutron-

612   scattering and electron-microscopy studies of the premartensitic phenomena in Ni_xAl_100-x

613   alloys, Physical Review, B, 44, 9301–9313.

614

615   Trepmann, C., and Stokhert, B.(2001) Mechanical twinning of jadeite – an indication of

616   synseismic loading beneath the brittle–plastic transition, International Journal Earth Sciences, 90,

617   4–13.

618

619   Tsatskis, I., and Salje, E.K.H. (1996) Time evolution of pericline twin domains in alkali

620   feldspars: A computer-simulation study, American Mineralogist, 81, 800-810.

621

622   Tsekenis G., Uhl J.T., Goldenfeld N., and Dahmen K.A.(2013) Determination of the universality

623   class of crystal plasticity , Europhysics Letters, 101, 36003.

624

625   Tullis, T.E. (1980) The use of mechanical twinning in minerals as a measure of shear stress

626   magnitudes, Journal Geophysical Research, 85, 6263–6268.

627

628   Van Aert,S., Turner,S., Delville,R., Schryvers,D., Van Tendeloo,G., and Salje, E.K.H. (2012)

629   Direct observation of ferrielectricity at ferroelastic domain boundaries in catio3 by electron

630   microscopy. Advanched Materials, 24, 523–527.

631

632   Vernon, R.H., and Paterson, S.R. (2008) How late are k-feldspar megacrysts in granites?, Lithos,

633   104, 327 – 336.

634

635   Vernon, R. H. (1999) Quartz and feldspar microstructures in metamorphic rocks, Canadian

636   Mineralogist 37, 513–524.

637

638   Viehland D.D., and Salje E.K.H. (2014) Emergent phenomena in domain boundary dominated

639   materials: adaptive structures and functional twin boundaries Submitted to Annual Review of

640   Advanced Materials

641

642   Wang,Y., Ren,X., and Otsuka, K. (2006) Shape memory effect and superelasticity in a strain

643   glass alloy, Physical Review Letters, 97, 225703.

644

645   Yokota H., Usami H., Haumont R., Hicher P., Kaneshiro J., Salje E. K. H., and Uesu Y. (2014)

646   Direct evidence of polar nature of ferroelastic twin boundaries in CaTiO3 obtained by second

647   harmonic generation microscope, Physical Review, B 89, 144109

648

649   Zaiser M.(2006)   Scale invariance in plastic flow of crystalline solids, Advaches Physics, 55,

650   185–245.

651

652   Zhang M.,Wruck B.,Barber A.G., Salje, E.K.H., and Carpenter, M.A. (1996) Phonon spectra of

653   alkali feldspars: Phase transitions and solid solutions , American Mineralogist, 81, 92-104.

654

655   Zhao Z., Ding X., and Salje E.K.H. (2015) Why most ferroelastic twin boundaries could be

656   polar, submitted to Physical Review B.

657

658   Zhao Z., Ding X., Lookman T., Sun J., and Salje E.K.H. Mechanical Loss in Multiferroic

659   Materials at High Frequencies: Friction and the Evolution of Ferroelastic Microstructures (2013)

660   Advanched Materials, 25, 3244–3248.

661

662   Zykova-Timan, T., and Salje, E. K. H. (2014) Highly mobile vortex structures inside polar twin

663   boundaries in SrTiO3 , Applied Physics Letters, 104, 082907.

664

665

30

666   Figures:
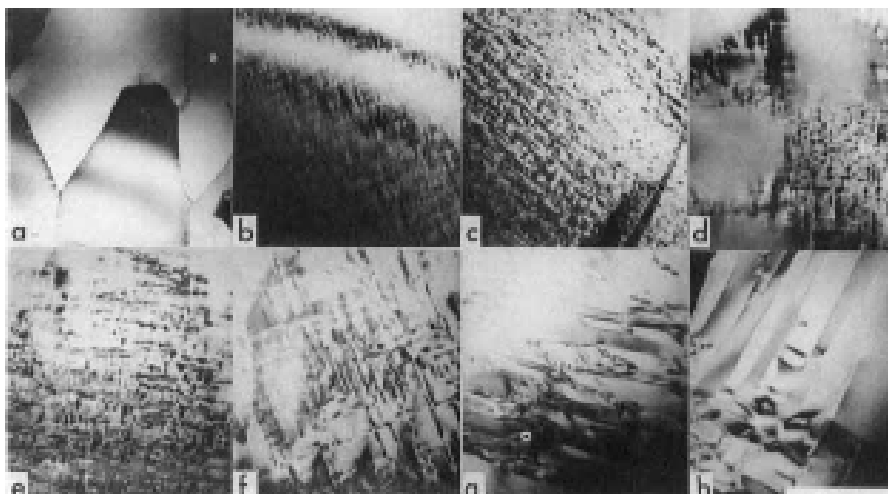
667
668

669   Fig. 1 Transmission electron micrographs illustrating the typical time evolution of

670   microstructures observed during the transformation from hexagonal to orthorhombic cordierite.

671   At 1673 K the transformation sequence is from (a) to (b), the finer scale of nucleation or

672   orthorhombic cordierite appearing to produce a continuously coarsening microstructure. The

673   length of the scale bar is 0. 2 μm. (after Putnis and Salje, 1994). Twins are seen in (a) and (h)

674   while tweed is typical for (b). The other images show mixtures between tweed and twins.

675   Cordierite is used as galls ceramics, e.g., cooking plates.

676
677
678
679

680

681

682

683
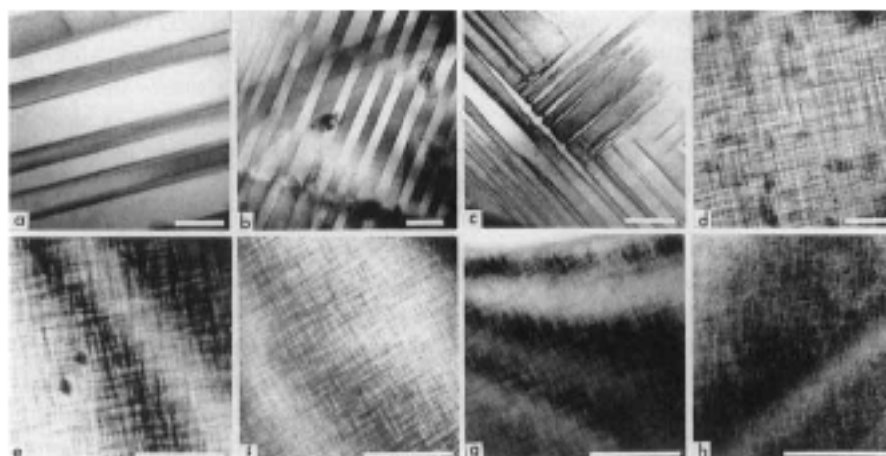
684

685

686   Fig. 2 Electron micrographs of {ll0}-type twin modulations in the high temperature superconductor

687    $YBa_2(Cu,Co)_3O_{7-\delta}$ with the incident beam parallel to [001]. Length of scale bar : 0.1 μm. The twin

688   structure transforms from a coarse twin (a) to a stripe pattern (b) and a junction pattern (c) to various

689   forms of tweed (after Schmahl et al., 1989).

690

691

692
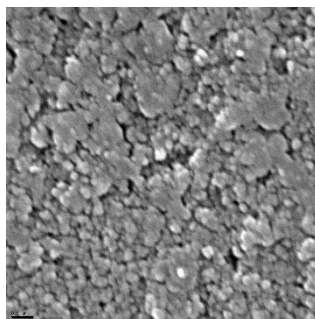
693

694

695   Fig.3 Porous structures in a synthetic SiO_2 glass, vycor, used in filters and glass ceramics (after Aufort at

696   al. 2014)

32

697
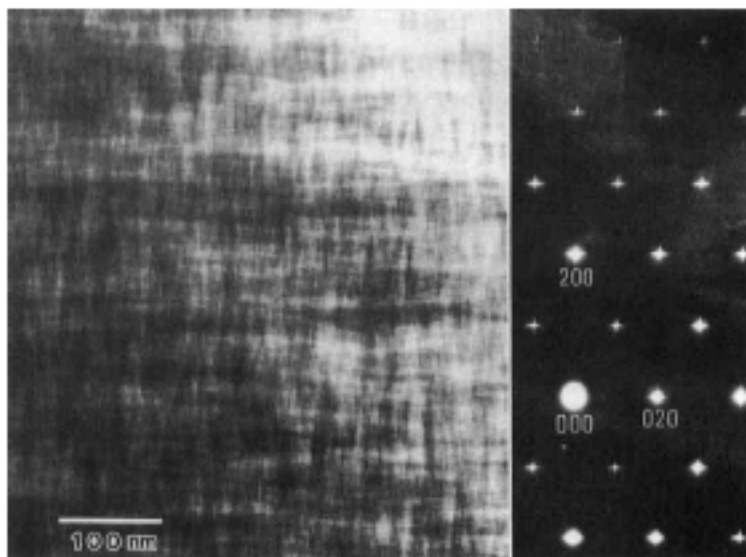
698

699   Fig. 4 Bright field transmission electron micrograph (and its associated electron diffraction pattern)

700   showing the tweed microstructure observed in K-feldspar (after McLaren and Fitzgerald 1987).

701

702

703

704
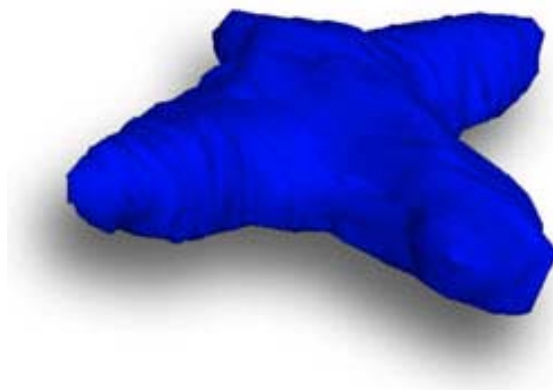
705

706   Fig. 5 Three dimensional representation of diffuse scattering profile associated with a tweed

707   microstructure in the superconducting oxide sample in Figure 2 (reanalyzed data from Locherer et al.

708   1998).

33
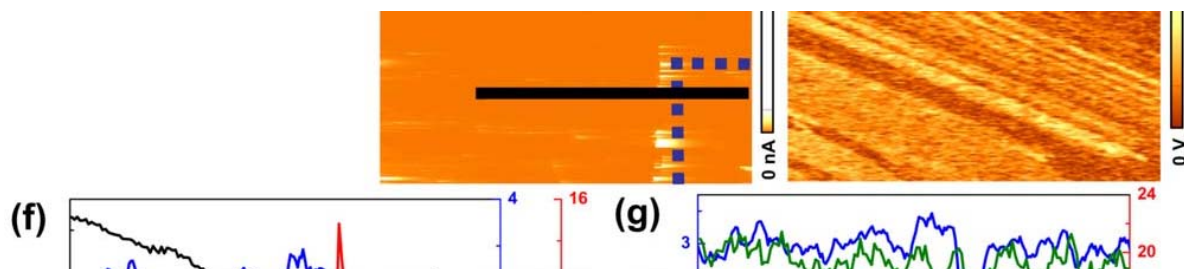
709

710   Fig. 6 Superconducting twin boundaries in WO$_3$ (after Kim et al. 2010) with the topological,

711   current and piezoelectric contrast across the same twin boundary.

712

713

714
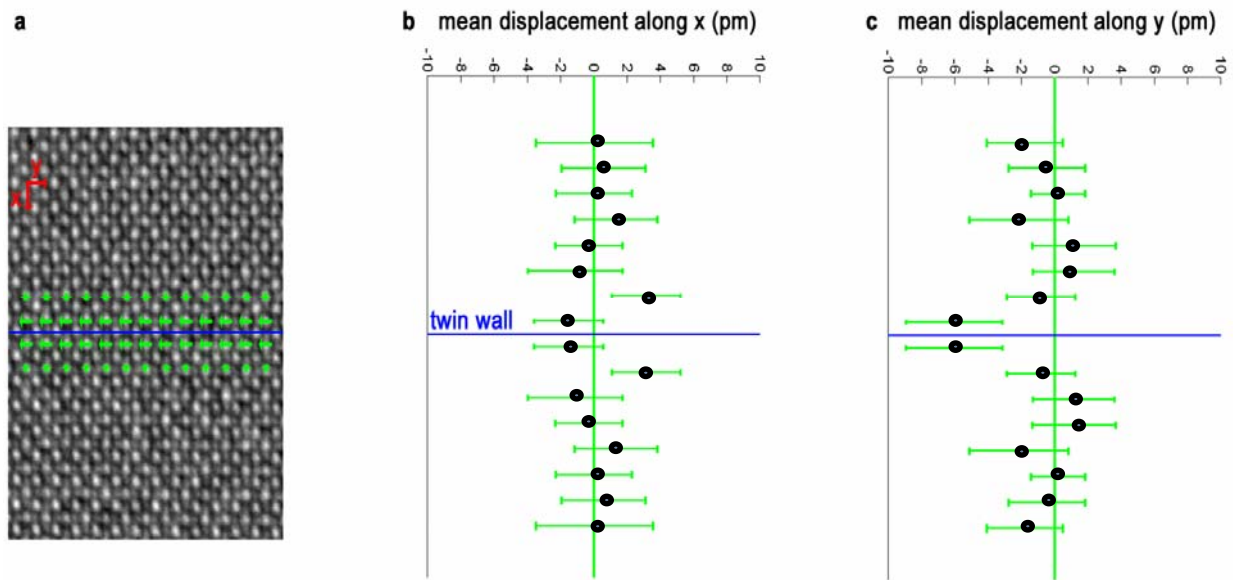
715

716 Fig.7 Polar twin boundaries in CaTiO$_3$. Displacements of Ti atoms near the twin boundary (a).

717 The blue horizontal line shows the position of the twin wall. b) Mean interatomic Ti–Ti column

718 distances perpendicular to the twin wall, averaged in the direction parallel with the twin wall,

719 together with their 90% confidence intervals. c) Mean interatomic Ti–Ti column distances

720 parallel to the twin wall, averaged in the direction parallel with the twin wall, together with their

721 90% confidence intervals (after Van Aert et al. 2012). The overall mirror plane symmetry of the

722 twin wall is preserved (Yokota et al. 2014))

723
724
725
726

727
728
729
730   Fig. 8 Phase diagram of phases with bi-quadratic coupling between order parameters and their

731   twin profiles. The relevant parameters are λ and κ, λ is the coupling strength and κ is the ratio of

732   the two characteristic length scales of the two order parameters (Salje 2012). Only the region $\lambda >$

733 -2, $\kappa > 0$ gives rise to interfaces between stable phases (after Conti et al. 2011).
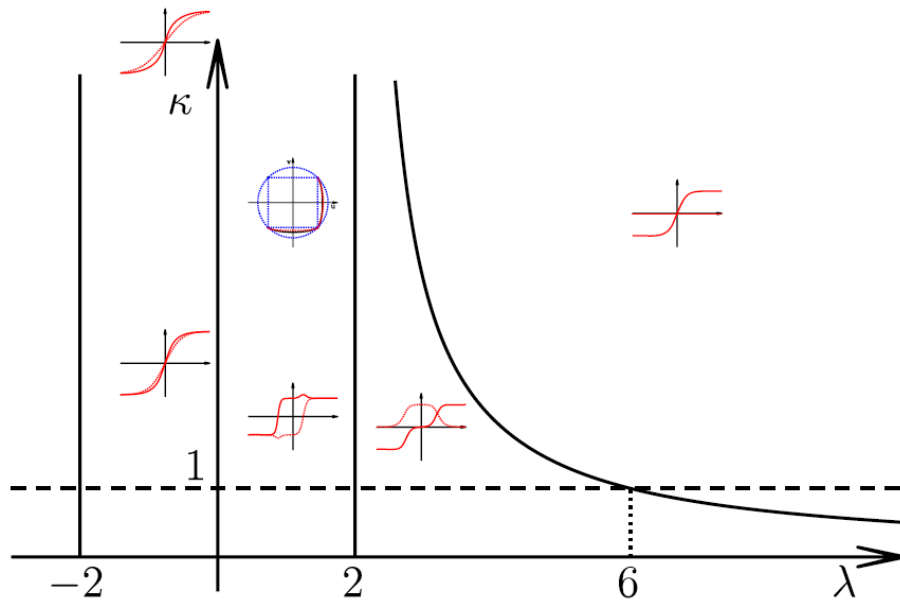
734
735
736
737
738
739
740
741
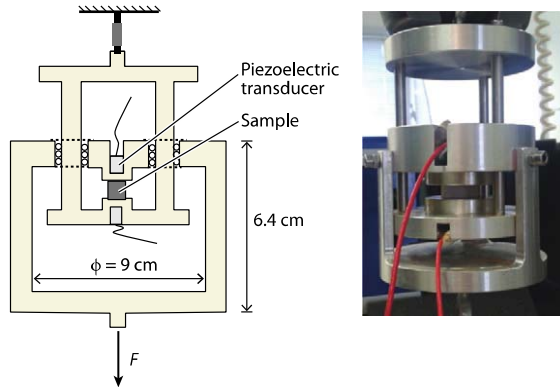
742
743
744   Fig.9 Experimental arrangement for measurements of the collapse under applied stress in porous

745   materials. The collapse is measured by the relative length change of the sample and by the

746   acoustic emission (AE) of jerks during the compression. The squared time derivative of the

747   length change $(dX/dt)^2 \square \, v^2$ is proportional to the acoustic activity (counts per second) so that

748   both data sets are used for the determination of the jerk statistics. The AE measures the energy

749   emission of the sample, which often follows a power-law distribution with exponent ε.

750
751
752
753
754
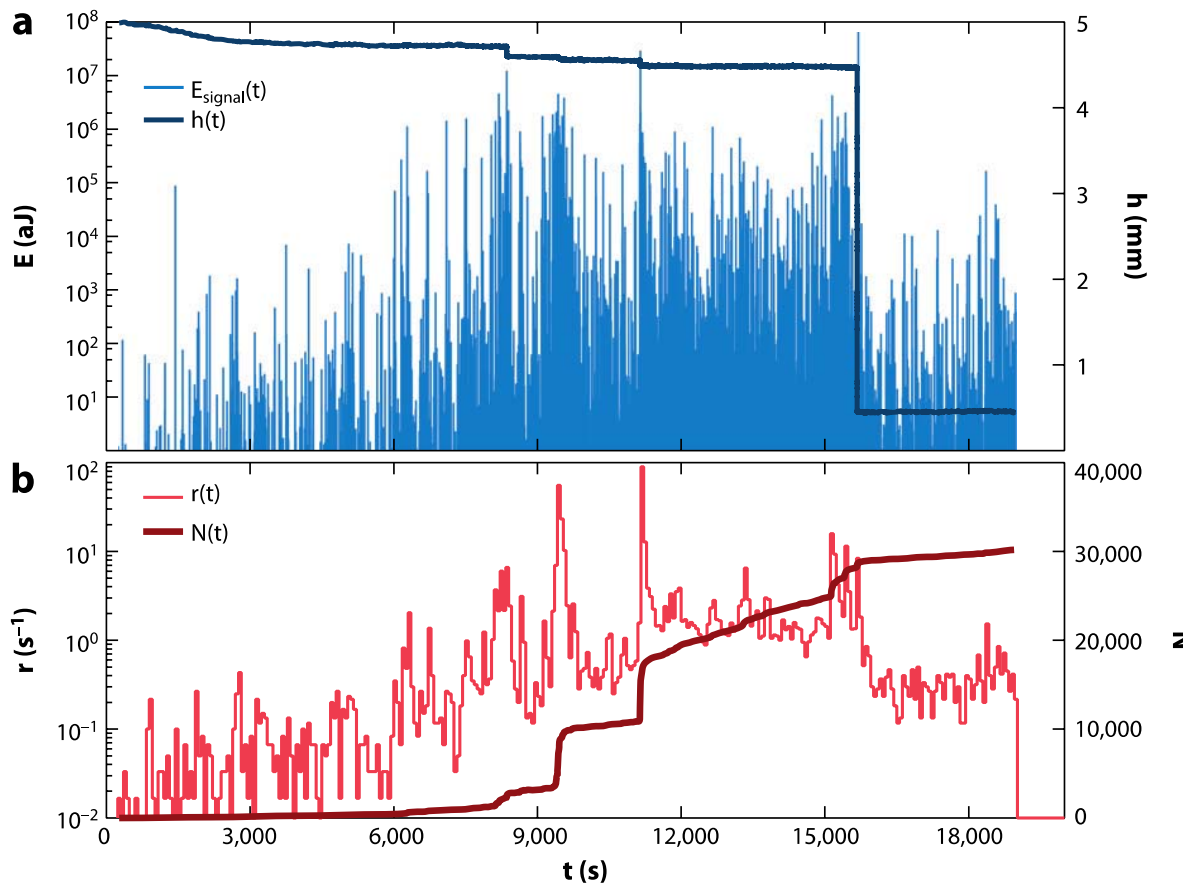
37

Fig.10 Typical compression jerk spectra as obtained by Baró et al. (2013). (a) The outcome of
compression on the specimen height (h) as a function of time (t) (time is proportional to stress, as
the experiment was undertaken under a constant stress rate) and the energy of the acoustic
emission (AE) avalanches, shown on a logarithmic scale. (b) Time evolution of the AE activity
rate and of the total number of events. Abbreviations: E_{signal} : acoustic emission energy,
h(t):height of the sample which shows the stepwise collapse, r(t): rate of the acoustic emission,
and N(t): accumulated rate of the acoustic emission. The difference between the reductions of the
height and the equivalent increase of the accumulated acoustic emission stems mainly from the
accumulated effect of pre- and after-shocks.
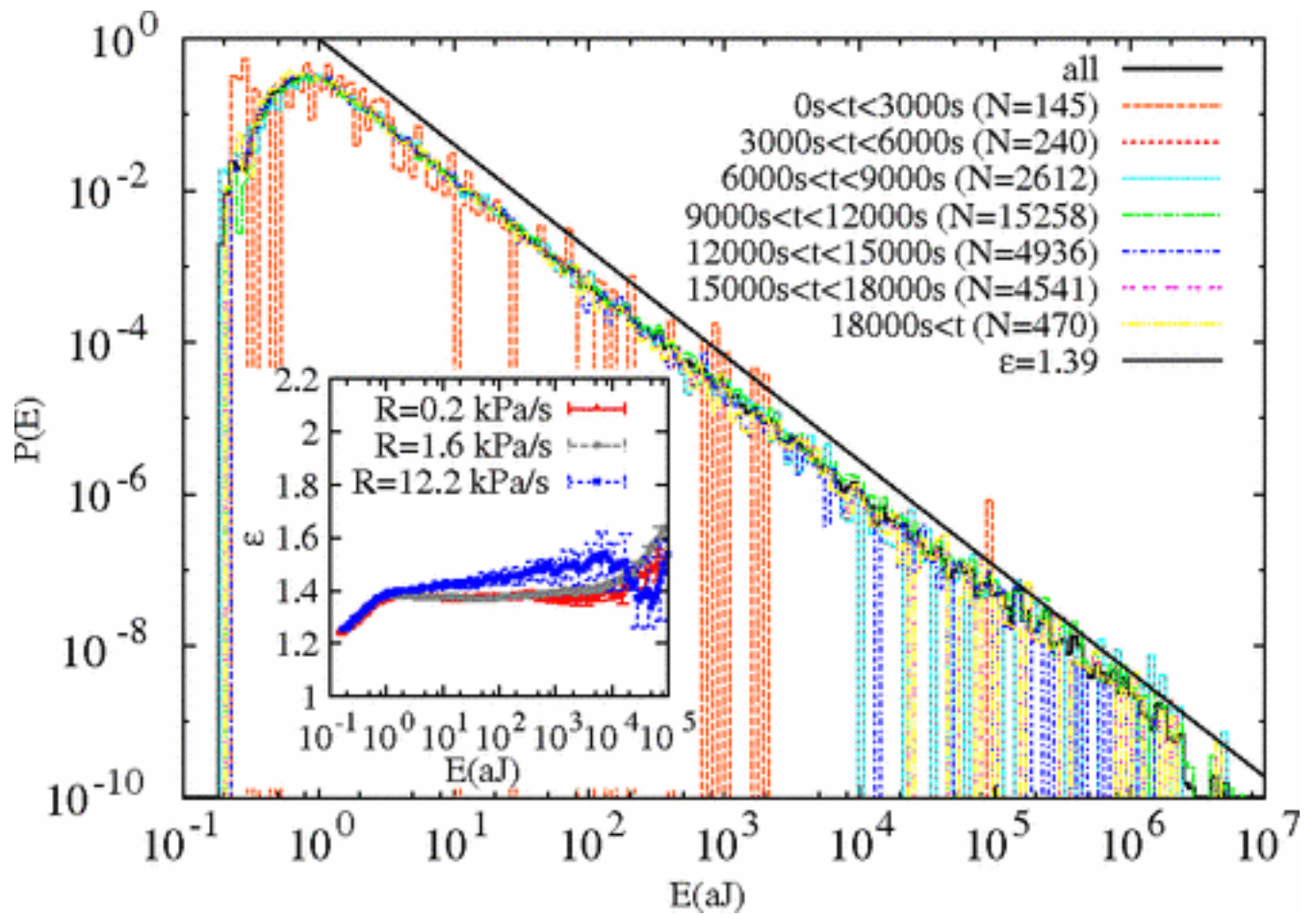
766
767
768
769   Fig.11 Distribution of avalanche energies during the full experiment with 7 different subperiods.

770   The line shows the behavior corresponding to $\varepsilon = -1.39$. The inset shows the ML-fitted exponent

771   as a function of a lower threshold E_{min} for the three experiments.

772
773

39

774
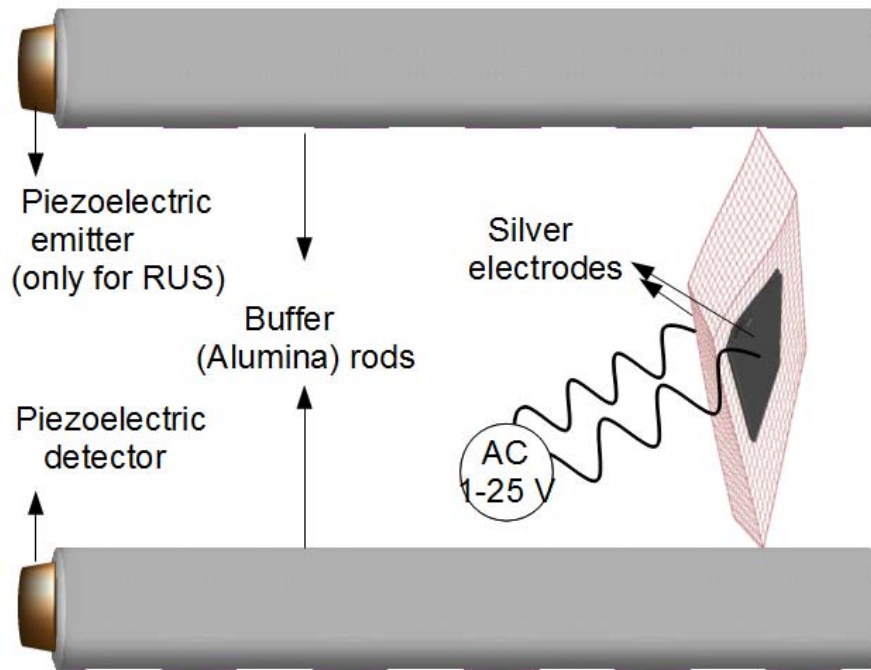
775   Figure 12: Schematic diagram of the experimental arrangement for resonant piezoelectric spectroscopy

776   (RPS). The same setup can be used for resonant ultrasonic spectroscopy (RUS) by applying the AC

777   voltage across the top piezoelectric transducer rather than the electrodes coating two parallel surfaces

778   of the sample. An AC voltage of 1-25 V is applied across the sample.

779
780
781
782
783
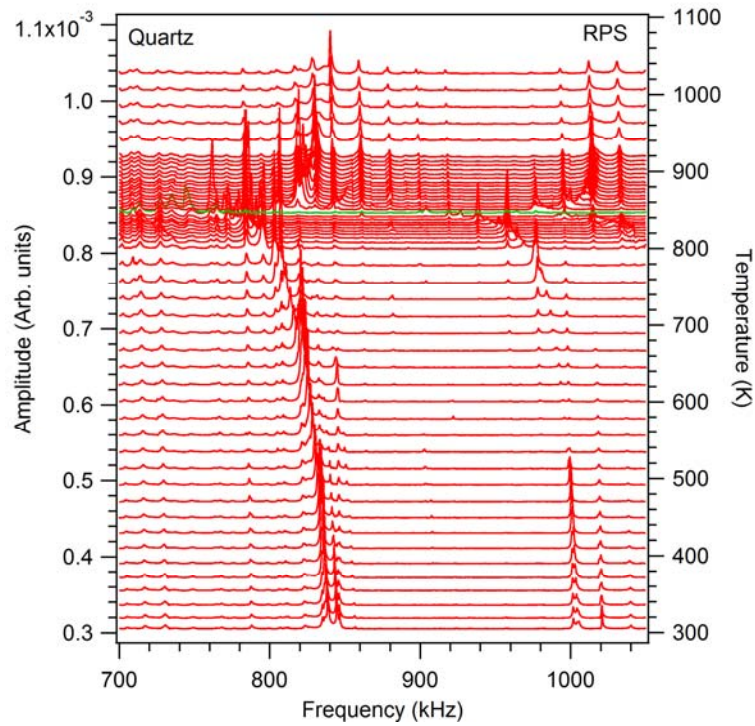
784

785   Figure 13: RPS spectra of quartz collected between 300 K and 1040 K. The spectrum shown in green is

786   assumed to be collected at T_c = 846 K. The left axis represents the amplitude. The spectra were translated

787   vertically in proportion to the temperatures at which they were collected so that the right axis represents

788   temperature.

789
790
791

792
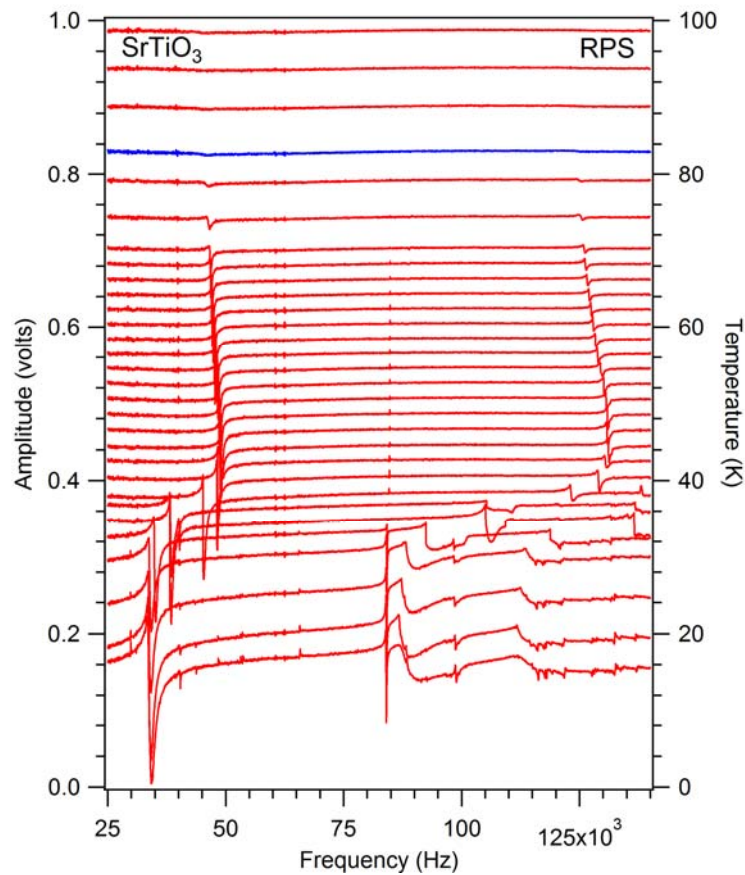
Figure 14: Low-temperature RPS spectra of $SrTiO_3$. Segments of RPS spectra in the frequency interval from 25 kHz to 100 kHz. The left axis represents the amplitude and the right axis gives the temperature at which each spectrum was collected. The spectrum shown in blue was collected at $T^* \sim 80$ K, below which $SrTiO_3$ shows piezoelectricity that originates from ferroelastic twin walls generated at the ferroelastic transition at 105K.
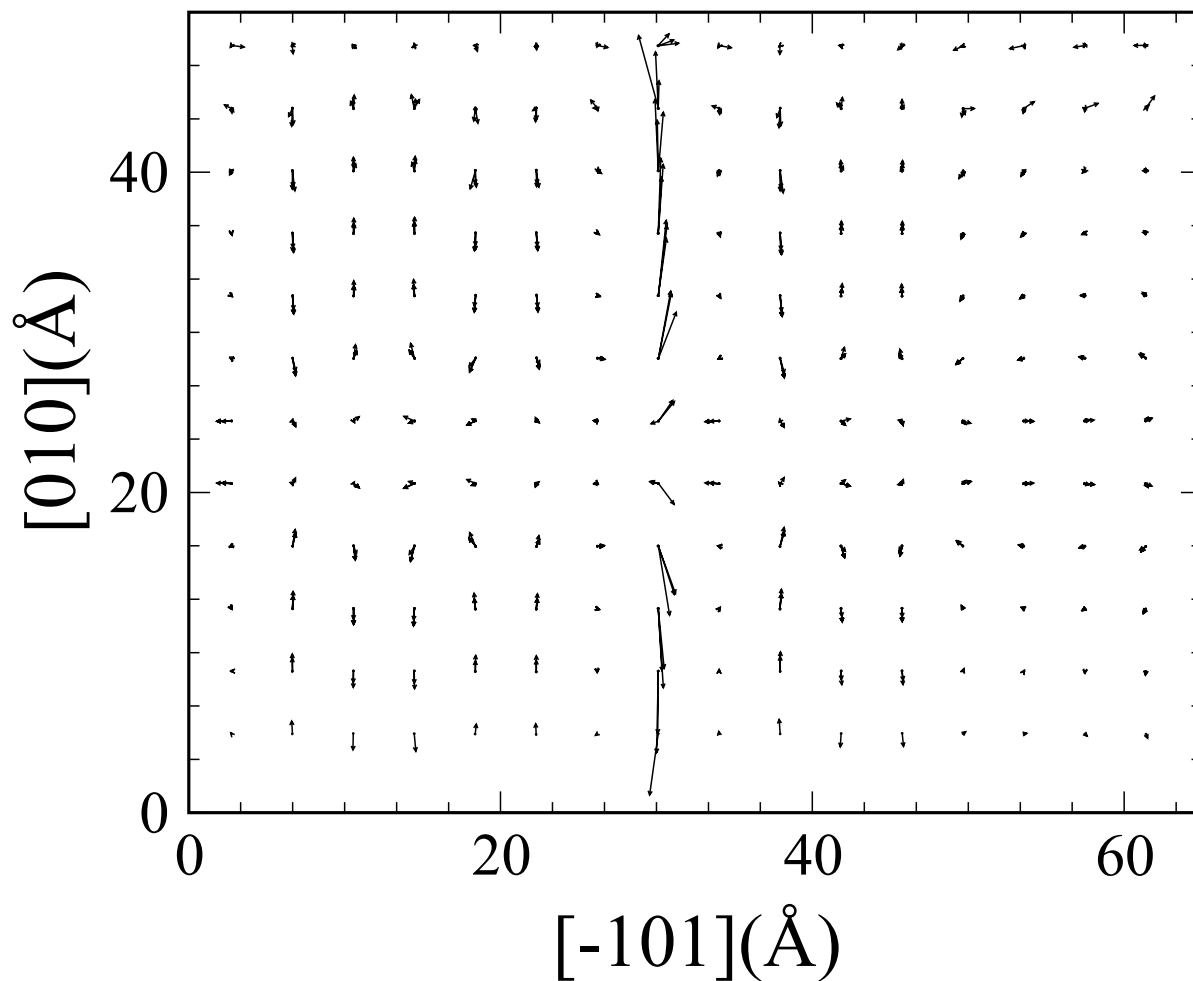
798

799

(a)

800

(b)
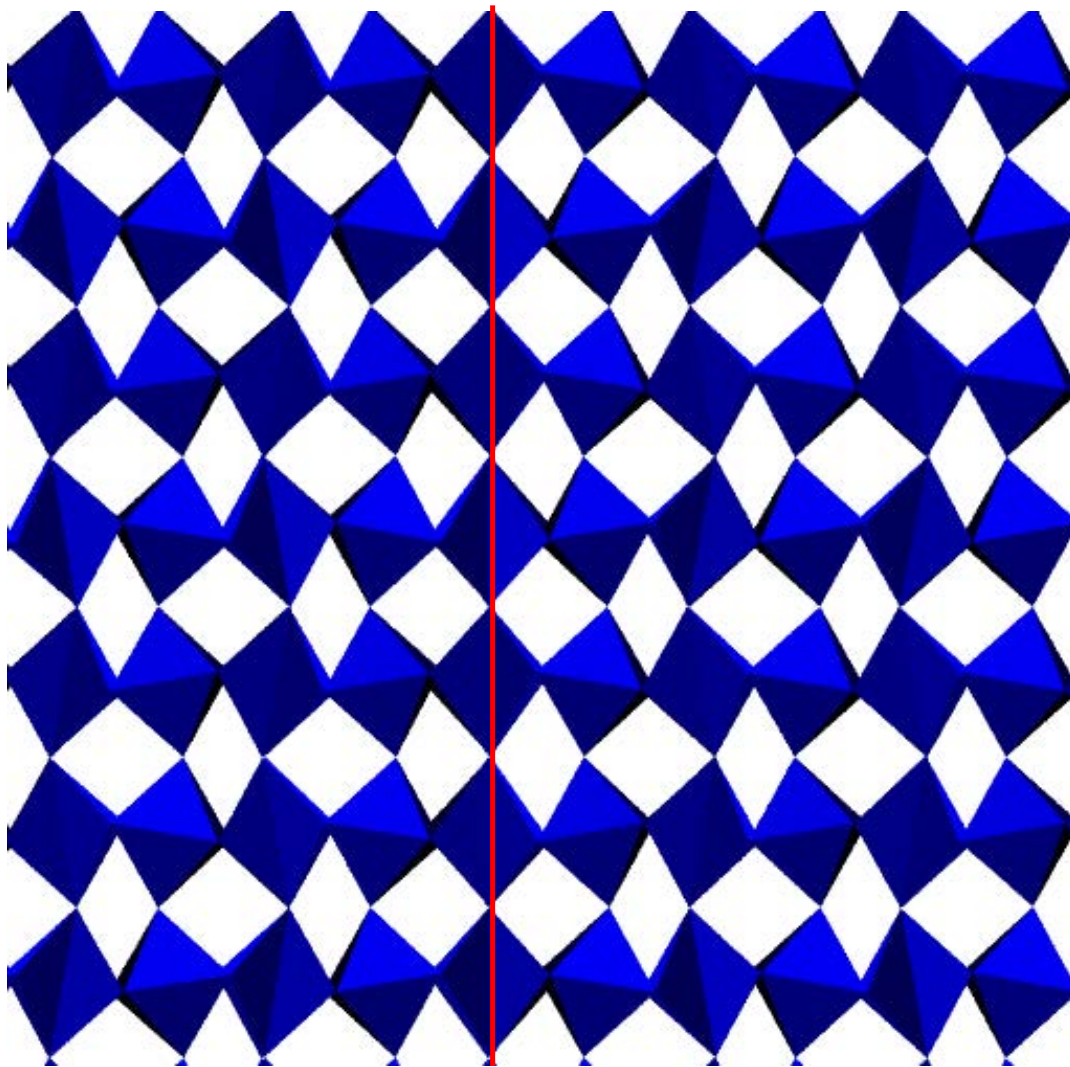
Fig.15. Twin structure of octahedral tilts in SrTiO3 (a) and the vortex structure of the Ti

off-centering in the twin wall and thermal fluctuations in the bulk.